Quantitative Flood Forecasting on Small- and Medium-Sized Basins: A Probabilistic Approach for Operational Purposes

FRANCESCO SILVESTRO AND NICOLA REBORA

CIMA Research Foundation, Savona, Italy

LUCA FERRARIS

CIMA Research Foundation, Savona, and DIST, University of Genoa, Genoa, Italy

(Manuscript received 5 November 2010, in final form 22 June 2011)

ABSTRACT

The forecast of rainfall-driven floods is one of the main themes of analysis in hydrometeorology and a critical issue for civil protection systems. This work describes a complete hydrometeorological forecast system for small- and medium-sized basins and has been designed for operational applications. In this case, because of the size of the target catchments and to properly account for uncertainty sources in the prediction chain, the authors apply a probabilistic framework. This approach allows for delivering a prediction of streamflow that is valuable for decision makers and that uses as input quantitative precipitation forecasts (QPF) issued by a regional center that is in charge of hydrometeorological predictions in the Liguria region of Italy. This kind of forecast is derived from different meteorological models and from the experience of meteorologists. Single-catchment and multicatchment approaches have been operationally implemented and studied. The hydrometeorological forecasting chain has been applied to a series of case studies with encouraging results. The implemented system makes effective use of the quantitative information content of rainfall forecasts issued by expert meteorologists for flood-alert purposes.

1. Introduction

Over the last few decades, much effort has been made in the field of flood prediction. The ground effects (e.g., floods, landslides) deriving from intense rainfall events can be devastating and very expensive in terms of the loss of human lives and damage to economic activities and assets.

In some regions the use of traditional alert systems based on rainfall observations, flood formation, and propagation modeling cannot be applied because of the very short watershed response times, which are often much shorter than what is necessary for starting up the ''machine of civil protection'' and its procedures. To overcome this problem, it is a common practice to resort to the use of numerical precipitation predictions issued by meteorological models as input for hydrological response models (e.g., Lin et al. 2002; Bacchi et al. 2002; Bartholomes and Todini 2005). Various works demonstrate that it is not possible to tackle the hydrological forecasting problem in a deterministic way (e.g., Krzysztofowicz 2001), and consequently they propose probabilistic approaches to properly account for the uncertainties in the hydrometeorological forecasting chain (Siccardi et al. 2005; Schaake et al. 2007; Verbunt et al. 2007; Cloke and Pappenberger 2009).

The two main sources of uncertainty associated with the meteorological input that have to be accounted for are 1) the uncertainties related to meteorological predictions and 2) the uncertainties due to the scale of inconsistencies between meteorological forecast input and hydrological response that arise when dealing with small- and medium-sized basins. In this last case, the different spatiotemporal scales between meteorological model outputs and hydrological model inputs can cause poor-quality streamflow predictions, even in cases where we have a perfect rainfall forecast for the spatiotemporal scales solved by a meteorological model (Ferraris et al. 2002). In this work, we do not consider the sources of uncertainty related to hydrologic modeling because they are at least one order of magnitude smaller than those associated

Corresponding author address: Francesco Silvestro, CIMA Research Foundation, via Magliotto 2, 17100, Savona, Italy.
E-mail: francesco.silvestro@cimafoundation.org

DOI: 10.1175/JHM-D-10-05022.1

with the meteorological forecast. We refer to Mascaro et al. (2010) and Zappa et al. (2011) for a complete description of this issue.

The literature that describes implementations of hydrometeorological prediction chains (e.g., Cloke and Pappenberger 2009) indicates that the most common option in accounting for the meteorological uncertainty is the use of precipitation predictions issued by ensemble prediction systems (EPSs). This framework cannot be the best option when dealing with predictions on very small catchments for two reasons. The first is that the output of an EPS needs a startup period of about 24 h to correctly reproduce the quantitative precipitation forecasts (QPF) uncertainty (Fundel et al. 2010; Marsigli et al. 2005); for this reason, we should use EPSs that are initialized at least one day before the forecasting time and that do not account for the latest atmospheric observations. The second is that, in order to cope with operational procedures and decision-making responsibility, hydrologists are allowed, in certain cases, to use ''certified'' predictions from (human) expert forecasters. These forecasters, on the basis of their knowledge, can analyze different meteorological models and estimate their reliability in different synoptic conditions and different local meteorological situations. This results in issuing a QPF that synthesizes a large quantity of information from synoptic to a very local scale.

In this work, we present the adaptation of a theoretical hydrometeorological forecasting system in an operational context designed for supporting decision makers in a civil protection system. The main goal is to quantitatively use the expert forecaster QPF as an input in the forecasting chain.

Two approaches are followed: the single-site approach for making predictions on medium-sized [$O(A) \sim 10^3$ km^2] basins and the multicatchment approach for small basin [$O(A) \sim 10^1$–10^2 km^2] forecasts. This procedure has been implemented in the Italian region of Liguria and is routinely used for civil protection purposes.

This paper is organized as follows: in sections 2 and 3, the general framework of the forecast chain and the territorial context are described. In section 4, the forecasting chain is contextualized within the framework adopted for the Liguria region. The application, the verification methodology, and the analysis of results are discussed in section 5, and discussions and conclusions are presented in section 6.

2. Probabilistic flood forecasting chain: General framework

The general framework of the probabilistic flood forecasting chain presented here is described in Siccardi et al. (2005). Because we are dealing with basins that have areas smaller than 10^4 km^2, three elements for our forecasting chain are needed. This can be understood through Fig. 1 (derived from Siccardi et al. 2005), which shows the different methodological approaches to use when producing hydrometeorological ensembles.

The first ingredient in the chain is the meteorological input, usually a QPF issued by either a meteorological model or by EPS prediction. The use of different meteorological scenarios issued by EPSs may help in accounting for the uncertainty in a QPF but usually only after a spinup time of about 24 h.

The second ingredient is a rainfall downscaling procedure that allows for generating high-resolution (1 km–10 min) ensemble rainfall forecasts starting from the QPF issued by the first element in the chain (meteorological prediction). The downscaling algorithm usually preserves the statistical properties of the large-scale field, such as the average precipitation amount and the position of large-scale precipitation structures, and creates small-scale precipitation fields with statistical properties similar to those observed from meteorological observations at midlatitudes (Ferraris et al. 2003). The third ingredient is a rainfall–runoff model needed to simulate the streamflow caused by the predicted precipitation event.

Depending on the catchment dimension and the temporal scale of its response, there are two possible approaches for the probabilistic forecast: single site and multicatchment. Siccardi et al. (2005) show that different types of hydrological forecast chains should be used (see Fig. 1), depending on the two ratios $l_{\text{met}}/l_{\text{hydro}}$ and t_c/t_s.

The term l_{met} is the typical reliable meteorological scale (Siccardi et al. 2005), which can range from 10 to 100 km, and l_{hydro} is the hydrological scale considered as the square root of the catchment area. The term t_c is the time scale of basin response, and t_s is the social response time to a civil protection warning that can be between 12 and 24 h.

For these reasons, when dealing with basins with an area of 10^3–10^4 km^2 ($l_{\text{met}}/l_{\text{hydro}} \sim 10^0 \div 10^1$), it is necessary to downscale the rainfall forecast issued by meteorological models or by EPSs and use it as input in the rainfall–runoff model for generating a series of discharge scenarios with related peak flow probability distributions. With this approach, a probabilistic discharge forecast can be obtained for each single catchment. This type of procedure is what is called a single-site approach.

When the target is the forecast in very small basins ($A \sim 10^1$–10^2 km^2 that correspond to $l_{\text{met}}/l_{\text{hydro}} \sim 10^1$–$10^2$ km^2), the single-site approach no longer represents the best option. The rainfall fields still need to be downscaled from the meteorological scale and used as input in a rainfall–runoff model. However, in this case it is impossible to evaluate which basins, belonging to a large region of l_{met}

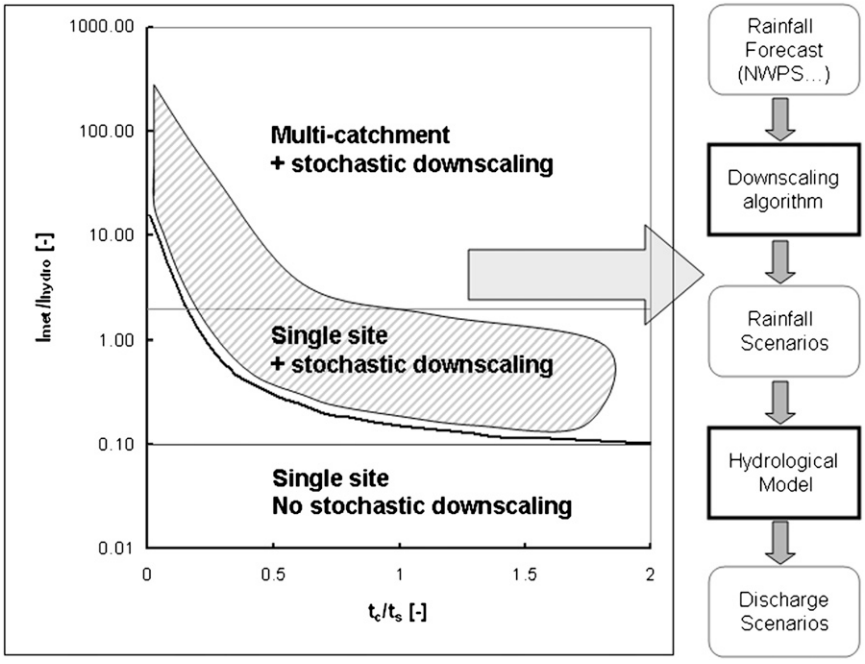

FIG. 1. Different methodological approaches to use when producing hydrometeorological ensembles at the varying of the scales of the processes involved. The variable t_s is the time scale of the social response of a population informed of a possible oncoming flood, t_c is the time scale of response of the analyzed basin, l_{met} is the space scale at which rainfall processes are satisfactorily represented by meteorological models, and l_{hydro} is the space scale that describes the analyzed hydrological basins. The area under the hyperbole-like curve identifies a domain that nowadays can be considered undefined, because of technical and scientific limitations in reliably forecasting precipitation on small scales in terms of both value and localization. The dashed area corresponds to the case of basins with area of order of magnitude from 10 to 10^4 km^2.

scale, will be affected by a flooding event. The forecasting procedure does not allow for any discrimination between one spatial localization and another, and therefore estimating the probability on a regional scale provides both useful and fundamental information for civil protection purposes. As a consequence, we cannot manage every single basin as an independent entity, so we must consider all the basins together inside the domain of l_{met} size. For this reason, we consider that the streamflow caused by a rainfall scenario on a particular catchment is representative of what could occur in one generic catchment inside the domain of size l_{met}. The results can be treated similarly to what is proposed by Boni (2000) in the regional analysis of peak discharge frequency for the Liguria region. The differences, which are due to morphological features of catchments of scale l_{hydro}, are overcome by introducing the flood index Q_{index} (Gabriele and Arnell 1991); the flows with return period T, indicated as $Q(T)$; and the growth factors $k_T = Q(T)/Q_{\text{index}}$. These elements can be derived from the statistical analysis of peak flows.

To formalize the multicatchment approach, we estimate the probability that, in at least one basin inside the domain of size l_{met}, the flow with a certain T is exceeded and so a certain k_T is exceeded too. Following this approach, the fact that a rainfall scenario causes the exceedance of a certain k_T in a particular basin is representative also of the other neighbor basins with similar hydrological response.

3. Territorial context

The Italian region of Liguria is a narrow strip of land about 250 km long and 20–30 km wide with a surface area of about 5421 km^2. It has very few flat areas and is covered mainly by forest. Most of the catchments have their outlet in the Mediterranean Sea and, because of the mountainous characteristics of the region, the main urban areas and towns have been established along the coast, often at the mouth of a river. This has elevated the risk of floods threatening lives and property. Another important fact that must be considered is that many basins have an area of less than 10^2 km^2. Only a few catchments have a drainage area over 200 km^2 with a response time to a rainfall event of just a few hours.

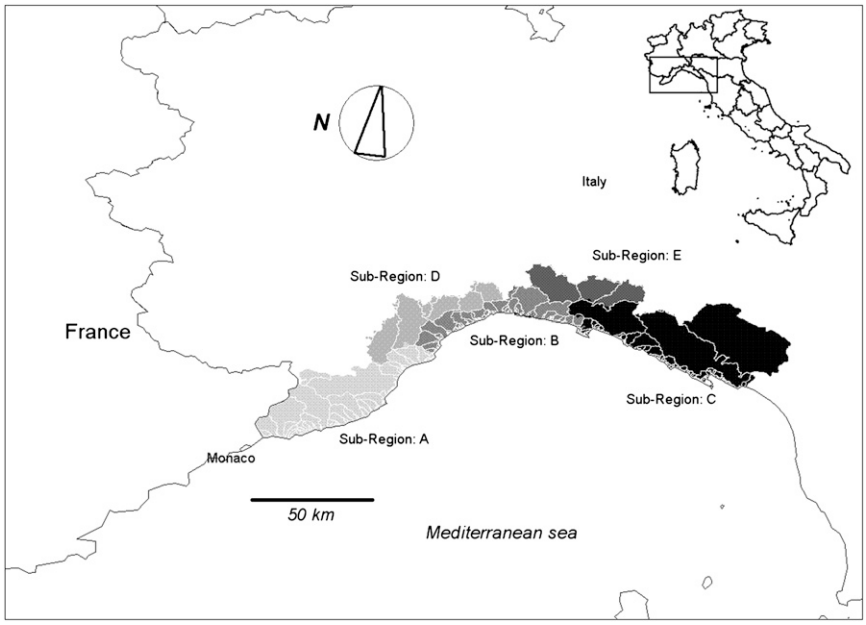

FIG. 2. Territorial context. The five alert subregions in the Italian region of Liguria are shown in different gray tones, together with the watershed of the main basins.

The Liguria region has a real-time meteorological network that provides a detailed set of meteorological variables. There are about 120 stations (each one provided with a rain gauge) with different sampling times ranging from 5 to 30 min.

The Hydro-Meteorological Monitoring Centre of Liguria Region (CMIRL) is the institution in charge of making hydrometeorological forecasts and it is responsible for the activities of nowcasting and the monitoring of rainfall events for civil protection purposes in the Liguria region. Liguria is divided in five alert subregions (Fig. 2) that correspond to five parts of the territory, and they are considered homogeneous from a meteorological point of view. They are divided into two groups: one group has three subregions with basins that have their outlets in the Tirrenic Sea (part of the Mediterranean Sea) and are called Tirreniche, and the other group has two subregions called Padane because their basins are in the mountainous part of the greater catchments that form the Padana Valley and the Po River.

4. The probabilistic flood forecasting chain in the Liguria region

a. Meteorological input: The subjective forecast

The implementation of a hydrometeorological forecasting system on small- and medium-sized basins commonly uses the deterministic or probabilistic precipitation forecasts issued by meteorological models (e.g., Taramasso et al. 2005; Rebora et al. 2006a; Cloke and Pappenberger 2009). During recent years, a new need has arisen among operational flood forecasters and that is the quantitative usage of expert forecast. This is because the forecasters, in order to reduce meteorological uncertainty, use various meteorological models for obtaining the final forecast. Regional forecasters also base their predictions on their knowledge of the territory, of its climatic peculiarities, and on the particular meteorological situation. All this leads to QPFs, made by regional forecasters, to be expressed in terms of accumulated rainfall on predefined areas and durations. These quantities usually depend on the context and the features of the region for which the forecasts are made. We refer to such a prediction as the ''subjective forecast.''

The CMIRL personnel use various meteorological models to make the subjective forecasts: the European Centre for Medium-Range Weather Forecasts (ECMWF) global circulation model, the limited area models Limited Area Model Italy (LAMI; Steppeler et al. 2003) and Bologna Limited Area Model (BOLAM; Buzzi et al. 1994), and a high-resolution limited area model called Modello Locale in *H* coordinates (MOLOCH; e.g., Diomede et al. 2008).

Statistical analysis of the extreme rainfall events in Liguria (Deidda et al. 1999; Boni et al. 2007) demonstrates that typical precipitation events associated with Mediterranean storms have durations of about 12–24 h. As already described, the regional catchments have a maximum dimension of about 10^3 km^2 that correspond to a concentration time (Maidment 1992) of about 10–12 h.

TABLE 1. Example of a subjective forecast for the five alert subregions in Liguria, which are named A, B, C, D, and E. Here, Pf_{12}, the maximum rainfall cumulated in 12 h on the alert subregion, is furnished together with the time the 12-h time window began, with respect to the reference instant of forecast (usually at 0000 LT of the day of forecast); Pa is the rainfall forecasted between the reference instant of forecast and the beginning of the time window of Pf_{12} (12 h per subregion); and Pf_3 (3 h per 100 km^2) is the maximum rainfall accumulated over 3 h on areas on the order of 10^2 km^2.

Forecast	Subregion A (mm)	Subregion B (mm)	Subregion C (mm)	Subregion D (mm)	Subregion E (mm)
Pf_{12} (12 h per subregion)	100	50	20	70	30
Pa	35	30	25	10	5
Pf_3 (3 h per 100 km^2)	60	60	60	60	60

Based on these considerations, a meteorological precipitation subjective forecast is issued and provides three quantities (see the example in Table 1):

1) The maximum average precipitation in a time window of 12 h for each homogeneous subregion (named Pf_{12}): To define this quantity a certain number of meteorological models are analyzed during the 12-h time window where the maximum precipitation amount is expected.
2) Once the Pf_{12} is defined, the meteorologist estimates the rainfall amount (Pb) that is expected between the reference starting time of the forecast (t_0) and the start of the 12-h window (t_{12}) associated with the maximum volume ($\tau b = t_{12} - t_0$). This is done for each subregion. The reference start time is the time at which the meteorologist starts his forecast and this is usually 0000 UTC on the day he makes the prediction.
3) The third parameter of the event is the maximum precipitation amount forecasted in a time window of 3 h and on areas of about 10^2 km^2 (named Pf_3). This number gives an idea of the local intensity of the forecasted event; high values means possible critical situations for basins with areas in the range 10^1–10^2 km^2. It indicates how much the precipitation volume, defined by Pf_{12}, tends to be concentrated in localized areas. A single Pf_3 is given for all the regional territory.

As can be seen, the subjective forecast, albeit represented by only a few numbers, has a large information content for various reasons: 1) it is derived from different meteorological models, 2) it is influenced by the experience of forecasters and by their knowledge of climatology and territory characteristics, and 3) it is tailored to the type of precipitation event and its interactions with the involved catchments.

b. Downscaling methodology: RainFARM

The downscaling procedure is crucial for generating an ensemble of precipitation fields that are consistent with large-scale predictions issued by meteorological models and/or by expert forecasters; it can reproduce the small-scale variability of precipitation needed to correctly force the rainfall–runoff model. The stochastic downscaling model accounts for the spatiotemporal variability of precipitation fields at scales smaller than those at which reliable quantitative precipitation forecasts are available.

In this part of the operational chain, Rainfall Filtered Autoregressive Model (RainFARM; Rebora et al. 2006a,b) has been used. This model is able to stochastically generate an ensemble of high-resolution precipitation fields by preserving the information at large scales derived from a quantitative precipitation prediction, and it is able to generate small-scale structures of precipitation that are consistent with radar observations of midlatitude precipitation events.

The basic idea is that the spatiotemporal Fourier spectrum of the precipitation field, estimated at large scale from a meteorological model prediction, follows the functional form

$$|\hat{g}(k_x, k_y, \omega)|^2 \propto (k_x^2 + k_y^2)^{-\alpha/2}\omega^{-\beta}. \quad (1)$$

Here, α and β represent two parameters of the model that are estimated from the power spectrum of precipitation predicted by a meteorological model on the wavenumbers–frequencies that correspond to the spatiotemporal scales at which the meteorological model prediction is considered reliable.

The spectrum defined by (1) can be easily extended over larger wavenumbers–frequencies, thus allowing for the generation of a spatiotemporal field at a higher resolution (Rebora et al. 2006a,b). The choice of random Fourier phases associated with the power spectrum (1) and the backward transformation in real space allows for generating a stochastic ensemble of high-resolution fields that are consistent at large scale with the QPF issued by numerical models.

RainFARM has been conceived for stochastically downscaling predictions issued by a meteorological model on a regular grid. However, in the operational framework presented here, we need to apply it to a precipitation

forecast issued as described in section 4a. To achieve this goal, we modify the original algorithm to allow for estimating the model parameters directly from the subjective forecast. In the next section, we explain how we adapted the original model in order to make it compliant with this new type of forecast output.

APPLICATION TO SUBJECTIVE FORECAST

When dealing with the downscaling of the subjective forecast previously described, the estimation of spectral parameters is not as straightforward as when a meteorological model output is used. As in Rebora et al. (2006b), we assume a power-law shape for the power spectrum; however, instead of estimating the slopes from the analysis of the power spectrum of numerical model precipitation prediction, we derive the two values of the slopes of spatial and temporal spectra (α and β) by comparing, for each alert subregion, the average precipitation Pf_{12} and the maximum Pf_3 as issued in the subjective forecast. The values of α and β observed for midlatitude precipitation events can range between -1.70 and -3.50 (i.e., between -0.70 and -2.50 if monodimensional average spatial spectra are considered).

We define a lookup table as one that, for each couple of possible values of Pf_{12} and Pf_3 given by subjective forecast, returns a couple of spectral slopes that allow for generating an ensemble of high-resolution precipitation fields. These fields have an average value over the alert subregion equal to Pf_{12} and maxima over 3 h and 100 km^2 that are, on average, equal to Pf_3.

To define the lookup table, we use a brute-force approach by generating $N = 10\,000$ downscaled fields for each value of Pf_{12} in a range between 5 mm (12 h)$^{-1}$ and 150 mm (12 h)$^{-1}$ and for each couple of spectral slopes (α and β) in the monodimensional range between -0.7 and -2.50. For each field generated with the set of three parameters α, β, and Pf_{12}, the maximum value over 3 h and 100 km^2 (Pf_{3i}, $i = 1, \ldots, N$) has been calculated. The fourth parameter needed for operational downscaling, Pf_3, has been estimated as the mean of Pf_{3i}.

At this point, we have defined a correspondence between Pf_{12} and Pf_3, issued by the forecasters, and the two spectral slopes. Given the two values of the prediction, we can derive the two optimal spectral slopes that guarantee the generation of an ensemble of high-resolution precipitation fields that are consistent with the forecaster's prediction both in terms of Pf_{12} and in terms of Pf_3.

Each final discharge scenario is composed of two parts. The first one has a constant intensity given by $Pb/\tau b$ (τb defined as in section 4a) and is common to all the scenarios, whereas the second is one of the downscaled precipitation scenarios generated starting from Pf_{12} and Pf_3.

c. Hydrological model: DRiFt

The hydrological model used in the system is a semidistributed (Giannoni et al. 2003) Discharge River Forecast (DRiFt) model (Giannoni et al. 2000, 2005). It has been designed for event-scale simulations and is based on a geomorphologic approach. It needs, as fundamental starting data, a digital elevation model by which the drainage network is individuated and every cell is classified as a channel or hill slope based on a filter that depends on drainage area and mean slope. Two different flow velocities are associated with channel cells and hill slope cells; as a consequence, the concentration time is defined for each point of the basin. The implemented infiltration scheme (Gabellani et al. 2008) allows the modeling of "multipeak" events making it possible to simulate quite long periods (5–8 days) during which different events can occur.

The runoff volume is routed to the outlet with a time variant T-hour Unit Hydrograph (TUH) technique, which, although representing the basin as a linear system, takes into account the spatial and temporal variability of the runoff production. Each cell that contributes to generate the basin response is considered separately from the others.

The discharge at any location along the drainage network is represented by the expression

$$Q(t) = \int_B M\left[t - \frac{d_0(x)}{v_0} - \frac{d_1(x)}{v_1},\ x\right] dx, \qquad (2)$$

where B is the drainage basin above the specified location, $M(t, x)$ is the runoff rate at time t and location x; $d_0(x)$ denotes the distances from x to the closest stream channel, $d_1(x)$ denotes the distance from the stream channel closest to x and the outlet, and v_0 and v_1 are the hill slope and channel velocities.

The hydrological model has been calibrated on the outlet sections where a hydrometric level gauge and reliable rating curve are available. The parameters on the other sections have been chosen on the basis of the calibration results and on both the authors' and CMIRL personnel's experiences (some examples in Gabellani et al. 2008; Giannoni et al. 2000, 2005). In Fig. 3 we report, by way of example, the simulation of the event occurred on 23 December 2009 in the calibrated outlet section Nasceto of Vara basin (202 km^2).

d. Forecast chain output: Single-site and multicatchment approach

The basins in Liguria have drainage areas that vary between 10 and 10^3 km^2. The applicable configurations of a probabilistic hydrological forecasting chain should

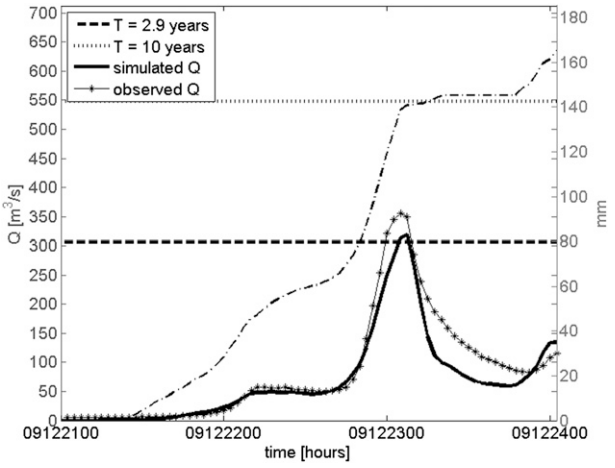

FIG. 3. Example of performance of hydrological model DRiFt. The simulated and observed discharge are reported for the outlet section Nasceto on Vara basin (202 km^2), together with cumulated rainfall along the period of simulation.

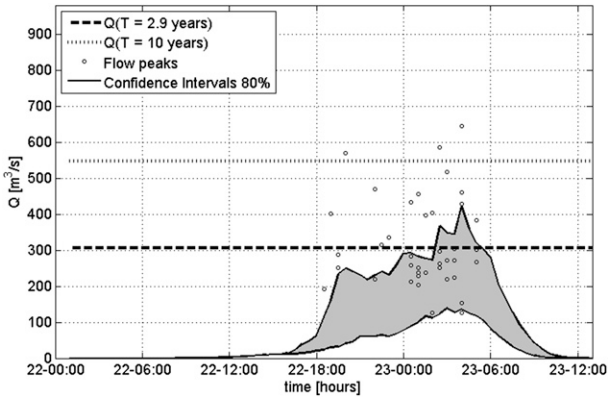

FIG. 4. Example of the single-site approach result: outlet section Nasceto on Vara basin (202 km^2). Forecast date is 22 Dec 2009. The points represent the peak flows of the forecasted scenarios derived by an ensemble forecasting, the gray area is delimited by 80% confidence intervals. The upper bound is 90th percentile, and the lower bound is 10th percentile. Values of Q with return periods of 2.9 (flood index) and 10 yr are reported.

be either the single-site approach with stochastic downscaling or the multicatchment approach with stochastic downscaling.

The civil protection rules define three different alert levels that depend on the criticality related to the forecasted event, level 0 (no alert), level 1, and level 2. From the point of view of the forecast system, the reference is to the return period of the peak flow. Two different return periods are related to the two alert levels, $T = 2.9$ yr (which is associated to the flood index) for alert level 1 and $T = 10$ yr for alert level 2. Otherwise, using detailed local knowledge, thresholds that are specific for certain outlet sections can be defined in order to have a forecast system that is not related to the return period but is based on the specific vulnerabilities of the catchment.

The statistical approach based on return period is useful because it permits the use of a homogenous system based on parameters that, when a frequency analysis of peak discharges is available, can be determined in all the basins of the region. In the case of Liguria, this analysis has been carried out by Boni (2000).

1) SINGLE SITE

The single-site approach is applied to catchments with a drainage area greater than 200 km^2 (with $l_{\text{hydro}} \geq 15$ km). Considering that the order of magnitude of homogeneous subregions areas is 10^3 km^2, l_{met} is about 30–40 km and the ratio $l_{\text{met}}/l_{\text{hydro}}$ is about 2. According to what is presented in Siccardi et al. (2005), the 200 km^2 area can thus be considered as the lowest dimension for which the single-site approach is valid.

The results of the single-site approach are shown in plots like Fig. 4. Time is shown on the x axis, whereas the y axis reports the discharge. This plot shows the peak flows related to the rainfall scenarios as dots, whereas the 80% confidence intervals, estimated at each time step, are reported as gray-shaded areas (Ramos et al. 2010). On the same graph, the threshold corresponding to alert level 1 (discharge with $T = 2.9$ yr) and alert level 2 (discharge with $T = 10$ yr) are reported.

The peak flow for each discharge scenario represents crucial information for decision makers, in particular when they are dealing with small- and medium-sized basins where the peaks distribution can be positioned far from confidence intervals in Q-time domain. The two forecast products, confidence intervals and peak flows, furnish different kinds of information and in such a way they are complementary; by showing both of them, it provides all the information needed about the forecast.

2) MULTICATCHMENT

The multicatchment approach is applied to basins with a drainage area smaller than 200 km^2 grouped in the five subregions as indicated in section 3.

The forecast is carried out for each subregion following these steps:

1) Rainfall scenarios are fed into the rainfall–runoff model and N_r discharge scenarios are generated for each of the N_b catchments within the subregion.
2) For each catchment, the peak flows of the discharge scenarios are extracted and divided by the catchment flood index (Q_{index}) derived from Boni (2000). As a result, $N_b \times N_r$ forecasted dimensionless growth factors k_T are obtained.

3) A value of return period T can be associated to each value of k_T. An $N_b \times N_r$ matrix of return times T is available.
4) A return period T^* is fixed, and the rainfall scenarios for which in at least one catchment an event with $T > T^*$ is expected are counted up. This number is indicated as $N(T > T^*)$.
5) The probability $P(T^*)$ that, in at least one catchment, an event with $T > T^*$ is expected is defined as $P(T^*) = N(T > T^*)/(N_r + 1)$. Note that, according to this procedure, it does not matter if a rainfall scenario generates one or more exceedances of T^*.
6) The steps 3–5 are repeated for different values of T^*.

The graphs in Fig. 5 show some examples of possible results of the multicatchment approach for a subregion; the x axis reports the return period T on a log scale, whereas the y axis indicates the probability $P(T)$. If the probability associated to a certain return period $T = T_1$ is $P = P_1$, it means that there is a probability P_1 that at least in one of the basins within the considered subregion the peak flow will exceed the flow with return period T_1 and a probability $1 - P_1$ that the peak flow will be lower than or equal to the flow with return period T_1.

The shape of this curve can give some information on the level of uncertainty associated with the forecast. When the curve has low slopes with a large range of T that correspond to nonnegligible probabilities, the uncertainty is high (dotted line in Fig. 5); if it tends to be step shaped, with a marked decrease after certain return periods, the forecast can be considered to be less uncertain (continuous line in Fig. 5).

e. *An index to evaluate the multicatchment forecast uncertainty*

A problem that can come up when the result of the multicatchment approach is available is the evaluation of the degree of uncertainty associated with the forecast. The result of the forecast is a curve that is not exactly a probability of exceedance because it measures the probability that, in ''at least one'' basin, the flow with a certain T is exceeded. The curve can have more than one T with $P(T) \sim 1$: for example, we can have $P(T = 2.9) \sim 1$, $P(T = 5) \sim 1$, and $P(T = 10) \sim 0.5$ (see the black continuous line in Fig. 5).

The operational application of the multicatchment approach is quite new, and decision makers may need a synthetic measurement of the uncertainty associated with this probabilistic prediction. The shape of this curve may help to estimate the level of uncertainty of the forecast, and the goal is to try to formalize it while considering the practical difficulties related to the curve interpretation.

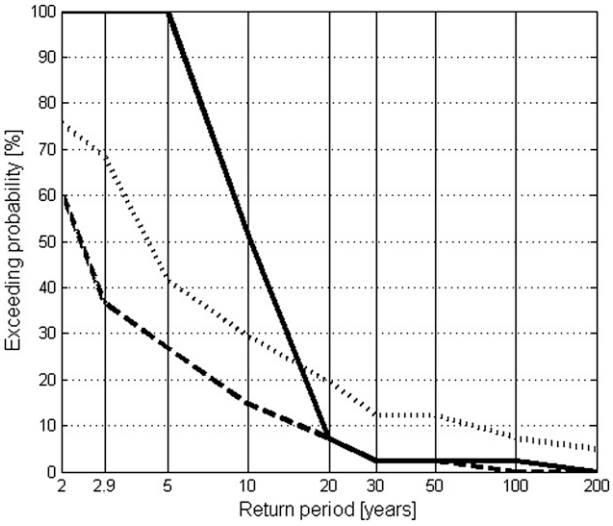

FIG. 5. Example of possible results deriving by multicatchment approach. Each line represents an example of a possible curve. In y axis the probability that at least one basin belonging to the alert subregion exceeds the flow with a certain return period T is reported. In x axis the return period is reported. The curve can have different shapes depending on the event type and the level of uncertainty of the forecast. When the curve has low slopes with a large range of T that correspond to nonnegligible probabilities, the uncertainty is high (dotted line); if it tends to be step shaped with a marked decreasing after certain return periods the forecast can be considered as less uncertain (continuous line).

We therefore defined a synthetic index that accounts for the uncertainty related to the multicatchment prediction, and we explain it by referring to Fig. 6. In this case, we use a linear scale for x axis to understand it better. We plot an example of forecast results, (i) a curve with probability $P(T) \sim 1$ from $T = 0$ yr to $T = 2.9$ yr that drops to 0 for $T = 50$ yr and (ii) an ideal perfect reference forecast represented by a step-shaped curve because it has substantially no uncertainty: the probability is $P(T) \sim 1$ when $T < T_s$ and then drops to 0. Here, T_s is defined as the return period for which $P(T_s) = 0.5$ on the real forecast curve. Referring to Fig. 6, we state that the dashed area is a measure of how much the real forecast differs from a perfect forecast. If we divide this quantity for the area under the real forecast, we obtain a variable that we call U_i and it varies from 0 (perfect and real forecasts coincide) to 1 (uncertainty tend to infinity). The discontinuity is positioned at T_s, chosen as T for which $P(T) = 0.5$, in order to minimize the dashed area for a given forecast. The choice of another $P(T_s)$ as reference can be made without changing the index meaning.

By indicating with $P_R(T)$ the function of a real forecast and with $P_P(T)$ the perfect forecast, it is possible to mathematically formalize the index as follows:

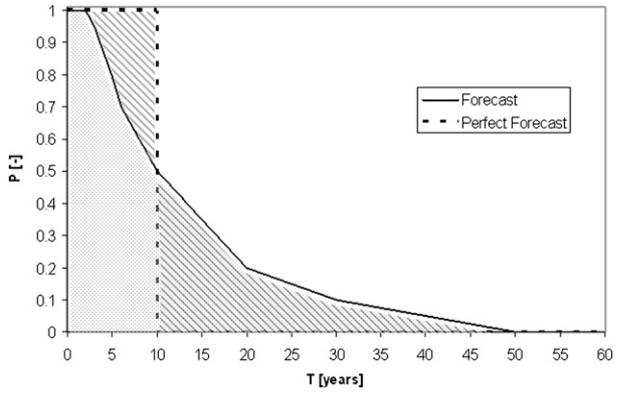

FIG. 6. Figure used for explaining the adopted uncertainty index U_i. The gray dotted area is the area bounded by the forecasted curve; the dashed area is the difference between the reference perfect forecast with no uncertainty and the forecasted curve, it is a measure of how much the forecast obtained by multicatchment approach differs from the reference forecast with no uncertainty.

$$U_i = \frac{\int_0^{T_S} [P_P(T) - P_R(T)]\,dT + \int_{T_S}^{\infty} P_R(T)\,dT}{\int_0^{\infty} P_R(T)\,dT}. \quad (3)$$

We had to use foresight because of the presence of events with very low severity: when as a result of the forecast $P(T = 2\ \text{yr}) \leq 0.5$ we set $T_s = T(P = 0.25)$, whereas, when $P(T = 2\ \text{yr}) < 0.25$, U_i is not calculated.

5. Case study

The hydrometeorological forecast chain presented in the previous sections has been running operationally at CMIRL since December 2008. Here it has been tested on a series of severe events that occurred between December 2008 and December 2009. The events for which both the maximum forecasted and observed accumulated rainfall in 12 h for all the alert subregions were less than 10 mm are not considered. A new statistical analysis should be performed once a larger number of events is available. Here, we consider eight severe events whose characteristics are reported in Table 2.

For each event N_r rainfall downscaled scenarios have been generated by using RainFARM. We chose $N_r = 50$ as a tradeoff between the computational performance of the system and the proper representativeness of the uncertainty due to the small-scale structure of the precipitation field. The discharge scenarios have been generated by feeding the RainFARM scenarios into the hydrological model DRiFt. There are $N_b = 83$ modeled outlet sections homogeneously distributed on the five alert subregions. For each event, the forecast system produces $N_b \times N_r$ discharge scenarios throughout the Liguria territory.

TABLE 2. List of considered events with the main characteristics in terms of Po_{12}, the maximum observed cumulated rainfall over 12 h on an alert subregion, and of Po_1, the maximum observed hourly intensity.

Event No.	Reference date	Max Po_{12} (mm)	Max Po_1 (mm h^{-1})
1	5 Dec 2008	56	18
2	20 Jan 2009	92	22
3	27 Apr 2009	66	24
4	9 Oct 2009	32	76
5	21 Oct 2009	102	60
6	28 Nov 2009	91	42
7	23 Dec 2009	78	52
8	25 Dec 2009	98	27

The single-site–multicatchment approaches are applied depending on the drainage area and on the response time associated to the considered outlet section. We selected the outlet sections with drainage areas of more than 200 km^2 and reliable discharge observations. For these pilot sites, the single-site approach has been tested. In addition, a comparison between observed and simulated discharge using precipitation observations has been made.

We then investigated the performances of a multicatchment approach. The forecast is made by building an exceeding probability curve for every event and for every alert subregion. To carry out the verification, we refer to the discharge simulations made with the hydrological model that uses observed rainfall as input; we consider them to be the ''truth,'' because discharge observations are available for only a few sections.

The scatterplot (Fig. 7) between observed (Po_{12}) and forecasted (Pf_{12}) precipitation amounts shows good performances of expert forecast. Although this is only one of the three ingredients in the meteorological subjective forecast, it is the most important because it defines the total volume of precipitation that is downscaled for obtaining the rainfall scenarios.

a. Single site

As stated in the previous sections, we apply the single-site methodology to catchments with areas larger than 200 km^2. In the Liguria region system, there are only four outlet sections with drainage areas between 200 and 1600 km^2 and with reliable and available observed discharge data. These sections are reported in Table 3 with their main characteristics and the section code that should be used as reference for the following figures.

Table 4 shows the results of the single site approach. The observed peak flows and the simulated peak flows obtained forcing the model with observed rainfall (Q_{pobs} and Q_{psim}) are reported, allowing for the evaluation of

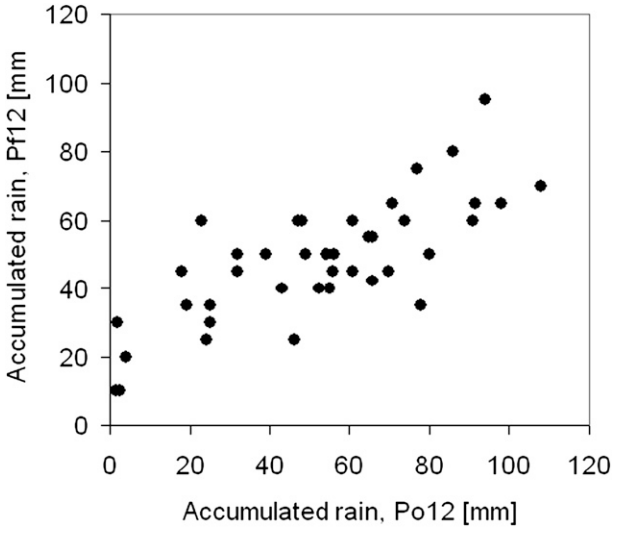

FIG. 7. Comparison between observed and forecasted rainfall for the eight events used as test cases. The variable is the maximum cumulated over 12 h averaged at a subregion scale. On x axis the observations (Po_{12}) are reported while on y axis the forecasts (Pf_{12}) are reported. The meteorologists furnish good forecasts, in general, but in some cases the difference between observation and forecast is not negligible and can reflect on the final quality of the forecast independently of the good intrinsic functioning of the hydrological forecast chain.

the hydrological model performances. As a term of comparison, we reported the maximum and minimum peak flows of forecast scenarios (Q_{pfMax} and Q_{pfMin}) and the mean of the corresponding peak flows distribution (Q_{pfMean}). The relative error of the forecasted 12-h maximum rainfall (Pf_{12}) on the subregion with respect to the observation is also shown (rainfall percentage error). As can be noted, Q_{psim} and Q_{pobs} are often very similar with percentage errors in most of the cases in a range between 2% and 20%. This is quite a good result considering that the used rating curves have an associated error of about 15%. In the case of Magra–Ponte della Colombiera outlet section, events with observed discharges smaller than 300 $m^3\ s^{-1}$ are very unreliable because the sea has far too much influence on the stream level and the corresponding observed flows are not realistic.

Looking at the forecast performance, it can be noted that frequently both Q_{psim} and Q_{pobs} have values between Q_{pfMax} and Q_{pfMin}, and often they are quite close to Q_{pfMean}. There are only a few cases where the simulations and observations are different to the expected values derived from the forecast chain. Most of these cases depend on the large differences between observed and forecasted rainfall input.

To show the results at a glance, Fig. 8 reports the box plot for each basin and for each event. The four plots report the event number on the x axis (see Table 2) and

TABLE 3. Basins to which the single-site approach has been applied with the main characteristics and the corresponding codes have been used in the figures.

Basin	Outlet section	CODE	Area (km^2)	Subregion
Arroscia	Pogli	PORTOV	201	A
Entella	Panesi	PANESI	364	C
Magra	Ponte Colombiera	PCOLOM	1650	C
Vara	Nasceto	NASCET	202	C

the discharge peaks on the y axis. The box plot whiskers indicate the maximum and minimum peak flows, the horizontal line in the box indicates the mean value and the box indicates the 25% and 75% quantiles. The black dot represents the maximum observed peak flow, and the diamond represents the flow obtained by feeding the rainfall–runoff model with the observed precipitation. The sketched and dotted lines represent $Q(T = 2.9\ \text{yr})$ and $Q(T = 10\ \text{yr})$. The general good performance is also shown by this representation, the observed peak flows are often between the 25% and 75% quantiles and they are out of the range individuated by maximum and minimum peak flows in only a few cases.

A particular case is the event number 4 (9 October 2009); it was a very localized event that caused relevant ground effects on only two adjacent small basins with areas of 22 and 30 km^2, respectively. In this case, the observed and simulated peaks were almost 0 for all of the four sections, and for this reason we did not report the results in Table 4. The results of the multicatchment approach show that this was a very uncertain event (Fig. 10). It is evident, when looking at box plots in Fig. 8, that there was a great variance with peak flows in a range from 0 to relevant values. This is because Pf_3 was very high in respect to Pf_12 and, as a consequence, RainFARM concentrated the volume on very small areas (less than 1 km^2), causing high hourly intensities that generate high and very localized runoff amounts. This reflects what really happened during the event. It is nevertheless evident that both the 25% and 75% quantiles correspond to low flow values.

A further test has been carried out to verify if the observed peaks have the same distribution as the forecasted ones. We considered the observed and forecasted peaks for all of the events and for all of the outlet sections and we normalized them with the flood index (Q_{index}) of the corresponding outlet section. We thus obtain a series of growth factors $k_T = Q(T)/Q_{\text{index}}$. The probability of exceedance curve has been built using the plotting position,

$$P(k_T > k_T^*) = 1 - \frac{i_{k_T}}{n + 1}, \tag{4}$$

TABLE 4. Single site forecasts and observations. The area is expressed in units of km^2 and discharge is expressed in m^3 s^{-1}. Only the basins hit by each event are considered. The terms Q_{pfMax}, Q_{pfMin}, and Q_{pfMean} are the maximum, minimum, and mean peak flows of the forecast discharge scenarios; Q_{pobs} and Q_{psim} are the observed and simulated peak flows; and the rainfall percentage error column is the percentage error of the forecasted maximum rainfall over 12 h on the subregion with respect to the observation.

Date	Section code	Rainfall percentage error (%)	Q_{pfMax}	Q_{pfMin}	Q_{pfMean}	Q_{pobs}	Q_{psim}
5 Dec 2008	PORTOV	300	65	25	37	20	10
	PANESI	−11	1000	130	450	113	143
	PCOLOM	−11	1700	710	1130	1100	1200
	NASCET	−11	450	70	200	265	230
20 Jan 2009	PORTOV	−19	430	67	140	95	110
	PANESI	−7	1510	270	660	640	630
	PCOLOM	−7	3670	1500	2300	2750	2780
	NASCET	−7	670	105	340	400	430
27 Apr 2009	PORTOV	−27	491	110	190	315	310
	PANESI	160	370	40	110	65	120
	PCOLOM	160	380	120	250	360	100
	NASCET	160	134	5	44	50	82
21 Oct 2009	PORTOV	28	290	3	70	8	10
	PANESI	2	530	15	120	195	190
	PCOLOM	2	580	120	315	430	300
	NASCET	2	186	6	60	25	1
28 Nov 2009	PORTOV	−37	260	3	65	100	129
	PANESI	−7	990	140	410	393	472
	PCOLOM	−7	1400	550	870	830	870
	NASCET	−7	385	47	167	163	135
23 Dec 2009	PORTOV	−16	400	40	100	200	160
	PANESI	−2	1200	310	630	450	600
	PCOLOM	−2	2800	1200	1800	2400	2500
	NASCET	−2	640	130	320	365	330
25 Dec 2009	PORTOV	−37	560	120	112	254	304
	PANESI	−7	2200	560	1050	860	830
	PCOLOM	−7	5700	2600	3700	3100	3400
	NASCET	−7	1100	260	600	400	350

where n is the dimension of the sample. Equation (4) represents the probability that the growth factor k_T is greater than k_T^*.

The observed and forecasted series are reported in Fig. 9 along with the Kolmogorov–Smirnov 95% confidence interval. The forecast sample size is higher than the observed one because for each section there are $N_r \times N_e$ samples, where N_e is the number of events. Figure 9 also shows that the observations belong to the population of forecasted peak flows. The observations always lay between the Kolmogorov–Smirnov confidence interval and, for $k_T > 0.7$ (i.e., $T > 2$ yr), they are fitted very well by simulated peaks. This means that the forecast discharge scenarios describe the observations well, particularly when we refer to the peak flows.

b. Multicatchment

The multicatchment approach is used for making streamflow predictions on catchments with areas smaller than 200 km^2. In the following we present the results for the eight severe events that were predicted and observed in Liguria during the considered period. The probability curves, similarly to those reported in Figs. 5 and 6, are represented, for one of the five subregions, in Fig. 10 (top) in a synthetic way. This gives the reader a prompt comparison between the predictive performances in different events. The x axis reports the reference number of the event, whereas the y axis reports the return period. A marker of a different shape for each probability level is set to the corresponding return period.

In the middle panel, a measure of prediction uncertainty is reported, which is called the uncertainty index U_i. As depicted in Fig. 6 and defined by (3), the larger the dashed area, the larger the uncertainty of the prediction compared to a ''perfect'' one (dashed line). According to (3), a value of $U_i = 1$ means complete uncertainty, whereas $U_i = 0$ means no uncertainty.

The operational use of this index is valuable because it gives a measure of the uncertainty associated with the lack of knowledge of the small-scale structure of precipitation as derived by a subjective forecast. The bottom panel shows the 12-h accumulated rainfall predicted over the area by the expert forecaster (Pf_{12}) compared to the 12-h rainfall observations for the event (Po_{12}).

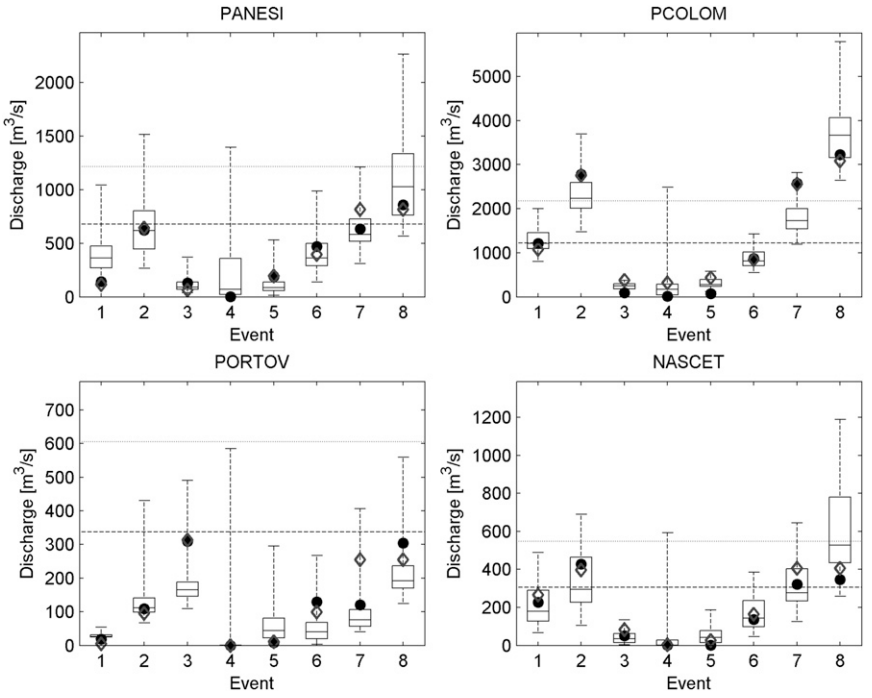

FIG. 8. Results of the single-site approach. The box plot for the 4 considered outlet sections are reported. The dots are the observed peak flows, the sketched and dotted lines are the flow with return periods 2.9 (flood index) and 10 yr.

In Fig. 10, we notice a good overall performance of the system. All the observed events fall inside the prediction interval ($0.95 < \text{Prob} < 0.05$), and there are no missed warnings. The exceeding probability curve in some cases is not very valuable because most of the observed events lay closer to a smaller return period than expected looking at intervals in the top panel. This is mainly due to the uncertainty in the prediction process. Consider, as an example, the prediction for event 4 (Fig. 10). The system predicts an event in this area that is potentially hazardous. In this case, $U_i \sim 1$ accounts for the low level of predictability of the event. It has to be noticed that, even for intense and well-predicted events, the values of U are not lower than 0.4–0.6. This is due to the residual uncertainty and accounts for the effect associated to the impossibility of knowing the exact structure of the precipitation field at small scales (1 km–10 min).

6. Discussion and conclusions

In this work, a hydrometeorological probabilistic forecasting chain has been designed and implemented. It is composed of 1) an expert forecaster's precipitation prediction as input, 2) a rainfall downscaling module (RainFARM), 3) a semidistributed hydrological model (DRiFt) and 4) a single-site–multicatchment postprocessing module. The forecast chain has been applied in the operational framework of the Liguria region civil protection system, using eight events as test cases. The characteristics of the territory and the dimension of the monitored basins does not allow for issuing discharge forecasts by using direct rainfall observations as input to an hydrological–hydraulic model for flow propagation nor does it allow for direct

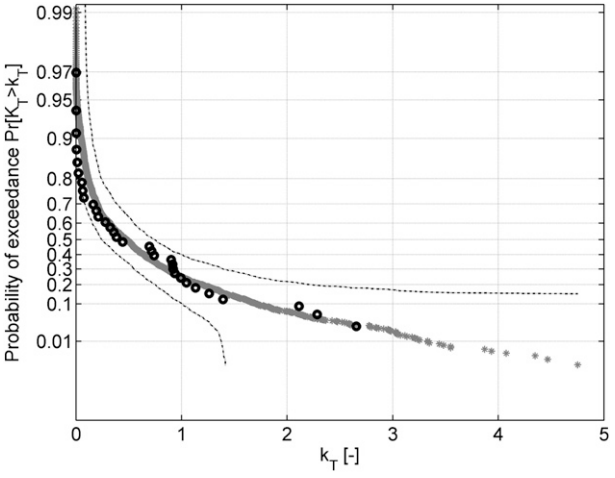

FIG. 9. Probability distribution of nondimensional observed and forecasted peak flows. The data from the four outlet sections used for single-site analysis are plotted. The black dots are observed flows, gray dots are forecasted flows, and sketched lines are the Kolmogorov 95% confidence intervals.

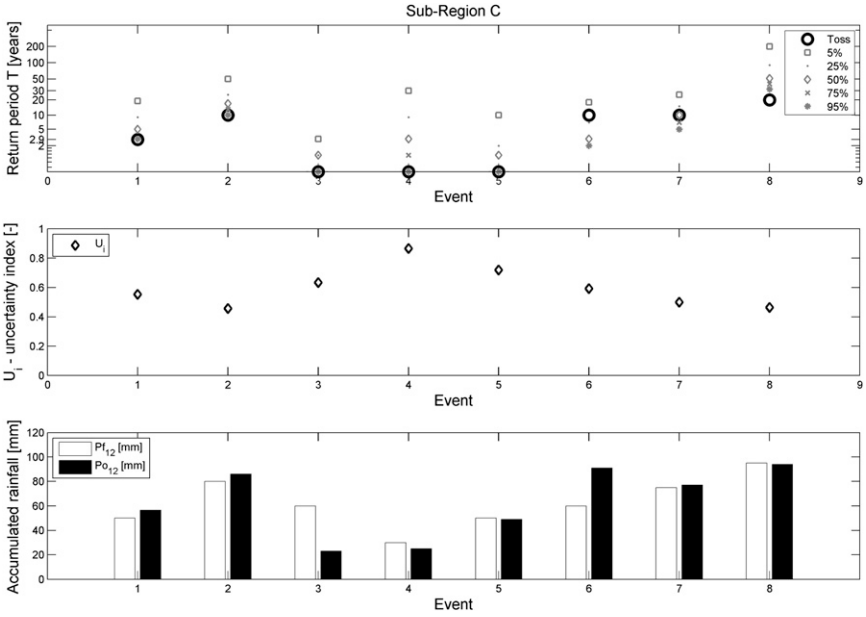

FIG. 10. Results of the multicatchment approach for the subregion A. On the *x* axis, there is the event number for all the subplots. (top) The return period on the *y* axis, where the different markers represent the various frequencies of exceeding and the circle is the maximum return period (in terms of peak flow) that occurred during the event. (middle) The uncertainty index on the *y* axis; it ranges between 0 and 1. (bottom) The maximum accumulated rainfall in 12 h over the subregion, where the white bars are the forecasts and the black bars are the observations.

coupling of meteorological predictions (used instead of rainfall observations) and hydrological models. For these reasons, it is obligatory to use rainfall downscaling procedures.

We focused the analysis on the use of a subjective forecast, which is a QPF given by a meteorologist who uses different meteorological tools together with his personal experience contextualized in a well-defined territory. The good performance of the methodology depends on the reliability of each single component: the subjective forecast quality, the downscaling methodology, and the hydrological model.

Rabuffetti et al. (2008) evaluated how uncertainty on QPF affects the reliability of a hydrometeorological alert system. If the rainfall input is dramatically different from the real occurrence, the performance of the chain will be of low quality. The subjective forecast in particular is given as a deterministic meteorological forecast, which summarizes all the analysis carried out by the forecaster. A possible improvement in the forecasting procedure could be the introduction of a methodology that accounts for the residual external uncertainty by giving a subjective forecast ensemble prediction or by associating a percentage error to the forecasted quantities.

The chain has been implemented following the single-site and multicatchment approaches described in Siccardi et al. (2005), and in both cases the results have a probabilistic nature. If discharge thresholds based on the specific condition of a basin are available, they can be introduced as a term of comparison in a single site analysis in order to evaluate the real effects of the predicted rainfall event.

Investigating the operational application of a multicatchment approach and the quantitative use of expert forecasts are the two main novel ideas in this work. For the estimation of a forecast degree of uncertainty, a new uncertainty index U_i has been introduced. Although the multicatchment approach gives a probability of occurrence for any return period T, the uncertainty index gives a measure of forecast uncertainty on a scale between 0 (certainty) and 1 (infinity uncertainty). For the analyzed events, U_i values 0.4–0.6 are associated to the less uncertain forecasts, but further analysis needs to be carried out. The analysis of the curve and of the uncertainty index can help the decision maker in the interpretation of the forecast.

The multicatchment approach appears to be a useful way of dealing with flood forecasting in regions with very small basins. Moreover, it seems to be a suitable tool to satisfy the civil protection when they need to issue a warning on a regional scale rather than on single basins.

The presented system can be adapted to different contexts when a forecast chain on small- and medium-sized

basins is needed. This specific chain uses DRiFt as the rainfall–runoff model, and it is suitable for orographically complex basins (see, e.g., Giannoni et al. 2000, 2005). The downscaling procedure also needs calibration based on the precipitation features in the given area.

The issue about the interpretation of the probabilistic chain results and the link with the final decision remains a matter for discussion. There is always a subjectivity factor that depends on the sensibility and experience of the hydrologist or the decision maker.

The probabilistic forecast gives, by definition, a number of possible scenarios and a probability that an event of a certain entity is likely to occur. Deciding whether to issue an alert depends on how much risk the decision maker is willing to take, and this in turn depends on the entity of damage and the danger to human lives.

The proposed approach allows the use of predictions issued by expert forecasters for an upcoming event and at the same time takes into account the uncertainties in ground effects due to small-scale spatiotemporal variability in the precipitation field. Many works have been devoted to the probabilistic approach in large-sized basins (e.g., Cloke and Pappenberger 2009, and references therein), whereas operational applications for small-sized basins are still not so common. As clearly demonstrated by Ramos et al. (2010), the probabilistic approach, albeit more powerful for characterizing the uncertainties in the prediction chain, is still not easily managed by an operational hydrological forecaster. Similar problems can be experienced when dealing with predictions on very small catchments.

Acknowledgments. This work is supported by the Italian Civil Protection Department and by Regione Liguria. We acknowledge Regione Liguria for providing us with the data from the regional meteorological observation network. We are very grateful to the meteorologists and the hydrologists of the Meteo-Hydrologic Centre of the Liguria Region for many useful discussions. We are grateful to Thomas Pagano and two anonymous referees for their helpful reviews and to Mike Whalley for his suggestions in reviewing the quality of the writing.

REFERENCES

Bacchi, B., A. Buzzi, G. Grossi, and R. Ranzi, 2002: Flood forecasting in a midsize catchment in the Southern Alps: Recent experiences on the use of coupled meteorological and hydrological models. *Proc. Second Int. Symp. on Flood Defence,* Beijing, China, IAHR, 965–972.

Bartholomes, J., and E. Todini, 2005: Coupling meteorological and hydrological models for flood forecasting. *Hydrol. Earth Syst. Sci.,* **9,** 333–346.

Boni, G., 2000: A physically based regional rainfall frequency analysis: Application to a coastal region in northern Italy. *Proc. First PLINIUS Conf. on Mediterranean Storms,* Maratea, Italy, European Geophysical Society, 365–376.

——, L. Ferraris, F. Giannoni, G. Roth, and R. Rudari, 2007: Flood probability analysis for un-gauged watersheds by means of a simple distributed hydrologic model. *Adv. Water Resour.,* **30,** 2135–2144.

Buzzi, A., M. Fantini, P. Malguzzi, and F. Nerozzi, 1994: Validation of a limited area model in cases of Mediterranean cyclogenesis: Surface fields and precipitation scores. *Meteor. Atmos. Phys.,* **53,** 137–153.

Cloke, H. L., and F. Pappenberger, 2009: Ensemble flood forecasting: A review. *J. Hydrol.,* **375** (3–4), 613–626.

Deidda, R., R. Benzi, and F. Siccardi, 1999: Multifractal modeling of anomalous scaling laws in rainfall. *Water Resour. Res.,* **35,** 1853–1867.

Diomede, T., and Coauthors, 2008: Discharge prediction based on multi-model precipitation forecasts. *Meteor. Atmos. Phys.,* **101,** 245–265.

Ferraris, L., R. Rudari, and F. Siccardi, 2002: The uncertainty in the prediction of flash floods in the northern Mediterranean environment. *J. Hydrometeor.,* **3,** 714–727.

——, S. Gabellani, N. Rebora, and A. Provenzale, 2003: A comparison of stochastic models for spatial rainfall downscaling. *Water Resour. Res.,* **39,** 1368–1384.

Fundel, F., A. Walser, M. A. Liniger, C. Frei, and C. Appenzeller, 2010: Calibrated precipitation forecasts for a limited-area ensemble forecast system using reforecasts. *Mon. Wea. Rev.,* **138,** 176–189.

Gabellani, S., F. Silvestro, R. Rudari, and G. Boni, 2008: General calibration methodology for a combined Horton-SCS infiltration scheme in flash flood modeling. *Nat. Hazards Earth Syst. Sci.,* **8,** 1317–1327.

Gabriele, S., and N. Arnell, 1991: A hierarchical approach to regional flood frequency analysis. *Water Resour. Res.,* **27,** 1281–1289.

Giannoni, F., G. Roth, and R. Rudari, 2000: A semi-distributed rainfall–runoff model based on a geomorphologic approach. *Phys. Chem. Earth,* **25** (7–8), 665–671.

——, ——, and ——, 2003: Can the behaviour of different basins be described by the same model's parameter set? A geomorphologic framework. *Phys. Chem. Earth,* **28,** 289–295.

——, ——, and ——, 2005: A procedure for drainage network identification from geomorphology and its application to the prediction of the hydrologic response. *Adv. Water Resour.,* **28,** 567–581.

Krzysztofowicz, R., 2001: The case for probabilistic forecasting in hydrology. *J. Hydrol.,* **249,** 2–9.

Lin, C., A. L. Wen, M. Bland, and D. Chaumont, 2002: A coupled atmospheric-hydrological modeling study of the 1996 Ha! Ha! River basin flash flood in Québec, Canada. *Geophys. Res. Lett.,* **29,** 1026, doi:10.1029/2001GL013827.

Maidment, D. R., Ed., 1992: *Handbook of Hydrology*. McGraw-Hill, 1424 pp.

Marsigli, C., F. Boccanera, A. Montani, and T. Paccagnella, 2005: The COSMO-LEPS mesoscale ensemble system: Validation of the methodology and verification. *Nonlinear Processes Geophys.,* **12,** 527–536.

Mascaro, G., E. R. Vivoni, and R. Deidda, 2010: Implications of ensemble quantitative precipitation forecast errors on distributed streamflow forecasting. *J. Hydrometeor.,* **11,** 69–86.

Rabuffetti, D., G. Ravazzani, C. Corbari, and M. Mancini, 2008: Verification of operational Quantitative Discharge Forecast (QDF) for a regional warning system—The AMPHORE case studies in the upper Po River. *Nat. Hazards Earth Syst. Sci.,* **8,** 161–173.

Ramos, M.-H., T. Mathevet, J. Thielen, and F. Pappenberger, 2010: Communicating uncertainty in hydro-meteorological forecasts: Mission impossible? *Meteor. Appl.,* **17,** 223–235.

Rebora, N., L. Ferraris, J. H. Hardenberg, and A. Provenzale, 2006a: Rainfall downscaling and flood forecasting: A case study in the Mediterranean area. *Nat. Hazards Earth Syst. Sci.,* **6,** 611–619.

——, ——, ——, and ——, 2006b: RainFARM: Rainfall downscaling by a filtered autoregressive model. *J. Hydrometeor.,* **7,** 724–738.

Schaake, J. C., T. M. Hamill, R. Buizza, and M. Clark, 2007: HEPEX: The Hydrological Ensemble Prediction Experiment. *Bull. Amer. Meteor. Soc.,* **88,** 1541–1547.

Siccardi, F., G. Boni, L. Ferraris, and R. Rudari, 2005: A hydrometeorological approach for probabilistic flood forecast. *J. Geophys. Res.,* **110,** D05101, doi:10.1029/2004JD005314.

Steppeler, J., G. Doms, U. Shättler, H. W. Bitzer, A. Gassmann, U. Damrath, and G. Gregoric, 2003: Meso-gamma scale forecasts using the nonhydrostatic model LM. *Meteor. Atmos. Phys.,* **82,** 75–96.

Taramasso, A., S. Gabellani, and A. Parodi, 2005: An operational flash-flood forecasting chain applied to the test cases of the EU project HYDROPTIMET. *Nat. Hazards Earth Syst. Sci.,* **5,** 703–710.

Verbunt, M., A. Walser, J. Gurtz, A. Montani, and C. Schär, 2007: Probabilistic flood forecasting with a limited-area ensemble prediction system: Selected case studies. *J. Hydrometeor.,* **8,** 897–909.

Zappa, M., S. Jaun, U. Germann, A. Walser, and F. Fundel, 2011: Superposition of three sources of uncertainties in operational flood forecasting chains. *Atmos. Res.,* **100,** 246–262, doi:10.1016/j.atmosres.2010.12.005.